Revealing the two-body ring-breaking dynamics of benzene in the $(C_6H_6)_2$, C_6H_6Ar, and C_6H_6Kr dimers

Xinyu Zhang,[1,2] Xinning Zhao,[1,2] Hui Liu,[1,2] Xitao Yu,[1,2] Dianxiang Ren,[1,2] Xiaoge Zhao,[1,2] Xiaokai Li,[1,2] Chuncheng Wang,[1,2] Qinxin Wang,[3] Sizuo Luo,[1,2,*] and Dajun Ding[1,2,†]

[1]*Institute of Atomic and Molecular Physics, Jilin University, Changchun 130012, China*

[2]*Jilin Provincial Key Laboratory of Applied Atomic and Molecular Spectroscopy, Jilin University, Changchun 130012, China*

[3]*School of Electrical and Information Engineering, Jilin Engineering Normal University, Changchun 130012, China*

(Received 26 January 2023; accepted 6 April 2023; published 17 April 2023)

The ring-breaking dynamics of C_6H_6 in its three dimers [$(C_6H_6)_2$, C_6H_6Ar, and C_6H_6Kr] are investigated by performing three-body coincidence measurements after interaction with a strong femtosecond laser. The measurements enabled the observation of three ring-breaking channels, resulting in products of $C_1H_3^+ + C_5H_3^+$, $C_2H_3^+ + C_4H_3^+$, and $C_3H_3^+ + C_3H_3^+$ with the neighbor ions. Additionally, kinetic energies from intra- and intermolecular fragmentation are extracted. By using the neighbor ion as a reference, it is found that the lifetimes of corresponding dissociation states have a significant impact on the final angular distributions of the fragments. The vibration excitation of molecules induced by neighboring ions during the repelling process alters the relative ratio between the three observed ring-breaking channels. By examining the ring-breaking dynamics of aromatic molecules in different environments, this study provides valuable insights into molecular fragmentation in complex systems.

DOI: 10.1103/PhysRevA.107.043115

I. INTRODUCTION

Atoms and molecules in clusters influence the dissociation of nearby molecules. They are named neighbor roles in the reactions within clusters [1–8]. Neighbor roles have been proven important during the Coulomb explosion (CE) of molecular dimers [6–12], and the ultrafast dynamics can be studied by using laser-induced Coulomb explosion (LICE) [7–9,13,14]. The potential energy curves (PECs) associated with the dissociation of N_2^{2+} are influenced by the presence of N_2^+ in $(N_2)_2^{3+}$, resulting in a shift in the kinetic energy release (KER) of fragments [6]. Moreover, the nearby CO^+ breaks the symmetry of the $X^3\Pi$ state of CO^{2+} during CE of CO dimer, leading to the observation of a new fast dissociation channel of CO^{2+} [7]. The barrier of PECs is reduced by the adjacent Ar^+ atom in the case of $(N_2Ar)^{2+}$, resulting in a shorter lifetime of the metastable molecular cation state and the formation of NAr^+ [3]. During the fragmentation of N_2O dimer, the previously forbidden dissociation path between $B^2\Pi$ and $^4\Pi$ of N_2O^+ becomes accessible in the presence of a charged neighbor, opening a new dissociation channel. The fragmentation dynamics of molecular dimer can be tracked in a femtosecond time-scale using pump-probe measurements [8]. However, the study of neighboring molecules on molecular dissociation is only limited to small molecules, and there has been no comparison made between different neighbors.

The dissociation of benzene (Bz) is a slow ring-opening process [15–21] compared to the intermolecular fragmentation process between molecules in a cluster. Research has been focused on molecular clusters formed by Bz molecules with other motifs, such as rare gas atoms (He, Ne, Ar, Kr) or molecules [22–28]. Recent studies have investigated the intermolecular charge decay (ICD) between Bz molecules or the CE between Bz-Ar or Bz clusters, enabling the reconstruction of the structures or charge distribution of the cluster [27–30]. Richardson *et al.* reported the observation of three ion pairs, $C_1H_3^+ + C_5H_3^+$, $C_2H_3^+ + C_4H_3^+$, and $C_3H_3^+ + C_3H_3^+$, with corresponding measured KERs in the breaking of a Bz molecule [15]. It was found that $C_1H_3^+ + C_5H_3^+$ proceeds partly through the formation of a metastable benzene dication with a lifetime of about 200 ns, while two channels leading to $C_2H_3^+ + C_4H_3^+$ and $C_3H_3^+ + C_3H_3^+$ fragments occur on a timescale less than 50 ns [15]. The appearance energies for these three channels have also been measured, with $C_1H_3^+ + C_5H_3^+$ appearing at 27.8 eV, and other dissociation channels such as $C_3H_3^+ + C_3H_3^+$ and $C_2H_3^+ + C_4H_3^+$ appearing at 29.5 and 30.1 eV [18,19]. The corresponding states have been assigned, which arise from the loss of one electron from the HOMO and the other electron from the HOMO-1 [16,20,31]. Additionally, it was found that the relative ratios between the three channels measured with photo-dissociation and collision by H^+ and Ar^{8+} are quite different [15,32]. The most likely dissociation channel in photo-dissociation caused by He(II) light is $C_1H_3^+ + C_5H_3^+$ [15], whereas the channel with $C_2H_3^+ + C_4H_3^+$ has the highest branching ratio in the ion collision experiment [32]. The process of ring-opening in molecules, such as the Diels Alder reaction, is of great interest in molecular dissociation. The ring first opens to a long C-H chain, and then the dissociation occurs through very complex multiple transition states [16,31].

*luosz@jlu.edu.cn
†dajund@jlu.edu.cn

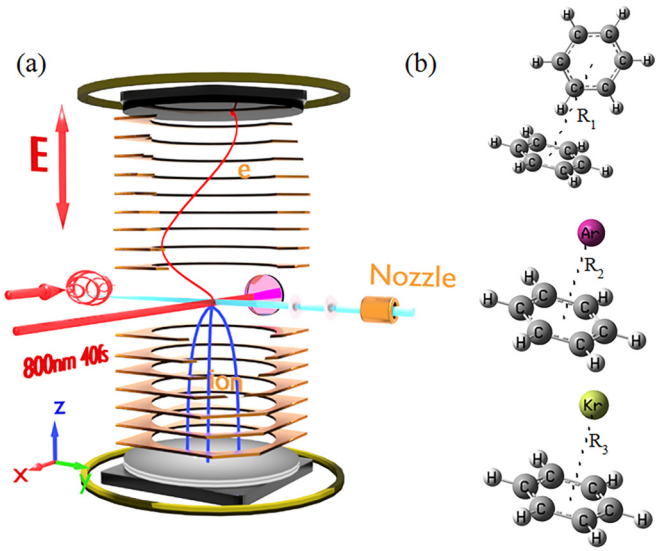

FIG. 1. (a) The experimental setup is illustrated schematically. (b) The structures of C_6H_6-Bz, C_6H_6-Ar, and C_6H_6-Kr, where R_1, R_2, and R_3 are the center-of-mass distance between two molecules and the surrounding molecule-atoms. The calculated distances are 4.8, 3.4, and 3.5 Å for three dimers.

In this paper, the ring-breaking of Bz in its three dimers, $(C_6H_6)_2$, C_6H_6Ar, and C_6H_6Kr has been studied by performing the three-body coincident measurement. The experiment identifies three two-body intramolecular CE channels, namely $C_1H_3^+ + C_5H_3^+$, $C_2H_3^+ + C_4H_3^+$, and $C_3H_3^+ + C_3H_3^+$ originating from $C_6H_6^{2+}$. Angular distributions of each channel are measured to examine the effect of dissociation state lifetimes by using neighbor ions as a reference. Additionally, the study explores the potential influence of repulsive neighbor ions on vibration excitation and how it may affect the branching ratios of the three channels.

II. EXPERIMENTAL METHODS

The three-body coincident measurements from CE of dimers are performed in cold-target recoil-ion-momentum spectroscopy (COLTRIMS) [33,34] and more details can be found in our previous works [27,35]. The experimental setup involved ionizing the dimers with a strong femtosecond laser (800 nm, 1 kHz, ~40 fs, 6×10^{14} W/cm^2) interacting with a supersonic target gas jet, as illustrated in Fig. 1(a). The $(C_6H_6)_2$, C_6H_6-Ar, and C_6H_6-Kr dimers depicted in Fig. 1(b) are generated by supersonic gas expansions of Ar (1.8 bar) and Kr (1.2 bar) with seeded benzene vapor at room temperature (~300 K). To minimize the possibility of preferred ionization of certain dimers inducing CE, a circularly polarized laser is employed to ionize three electrons sequentially [9]. The resulting ionic fragments are directed towards a delay-line detector that is both time- and position-sensitive for coincidence measurement, with the aid of a static electric field (19.8 V/cm). From the information gathered on flight time and position, the momenta and kinetic energies of each fragment ion are determined. The energy resolution is approximately 0.2 eV when the KER is less than 6 eV. The count rate is restricted to less than 0.4 per laser pulse, and only three-body coincidence events that comply with momentum conservation rules are selected from all detected particles.

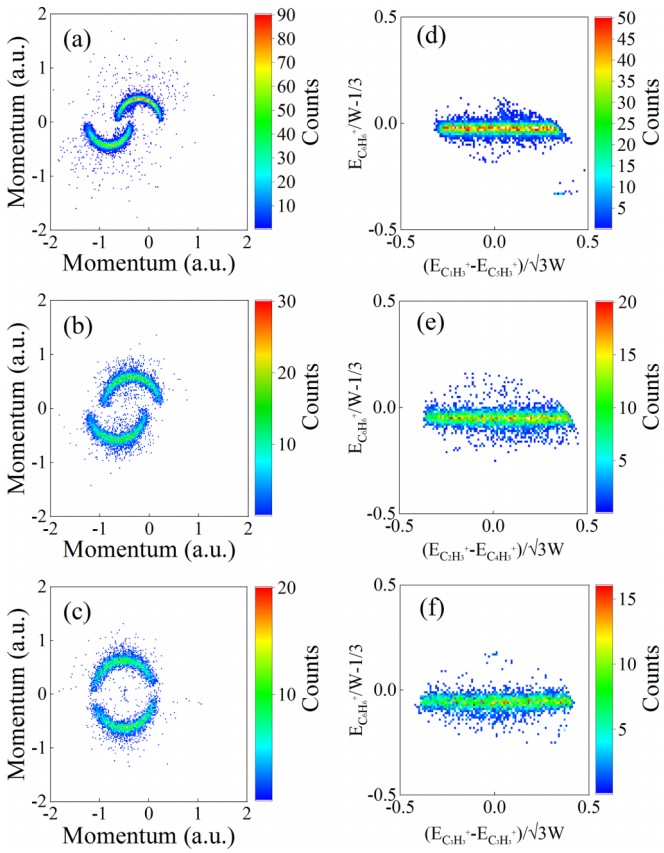

FIG. 2. The Newton plots for three fragmentation channels of the benzene dimer are shown in (a)–(c). (a) (1,3) + (5,3) channel, (b) (2,3) + (4,3) channel, and (c) (3,3) + (3,3) channel. The momentum of the Bz^+ fragment ion is rotated to the horizontal axis for normalization, and the momentum of the $C_1H_3^+$, $C_2H_3^+$, and $C_3H_3^+$ fragment ions is rotated to the vertical axis, with the Bz^+ ion placed at the coordinate axis. The Dalitz plots for the three dissociation channels with Bz^+ as adjacency are shown in (d)–(f).

III. RESULTS AND DISCUSSION

Three-body CE channels from $(C_6H_6)_2$, C_6H_6Ar, and C_6H_6Kr dimer are measured coincidentally when $C_6H_6^+$ (Bz^+), Ar^+, and Kr^+ are adjacent to the breaking of $C_6H_6^{2+}$:

$$[C_6H_6\text{–}Bz]^{3+} \longrightarrow C_6H_6^{2+} + Bz^+ \longrightarrow C_mH_3^+ + C_nH_3^+ + Bz^+, \quad (1)$$

$$[C_6H_6\text{–}Ar]^{3+} \longrightarrow C_6H_6^{2+} + Ar^+ \longrightarrow C_mH_3^+ + C_nH_3^+ + Ar^+, \quad (2)$$

$$[C_6H_6\text{–}Kr]^{3+} \longrightarrow C_6H_6^{2+} + Kr^+ \longrightarrow C_mH_3^+ + C_nH_3^+ + Kr^+, \quad (3)$$

where m and n are the number of C atoms, $m + n = 6$, and channels of $(1, 3) + (5, 3)$, $(2, 3) + (4, 3)$, and $(3, 3) + (3, 3)$ are abstracted for CE channels (1)–(3). The Newton diagrams of three fragment ions after CE of $[C_6H_6 - Bz]^{3+}$

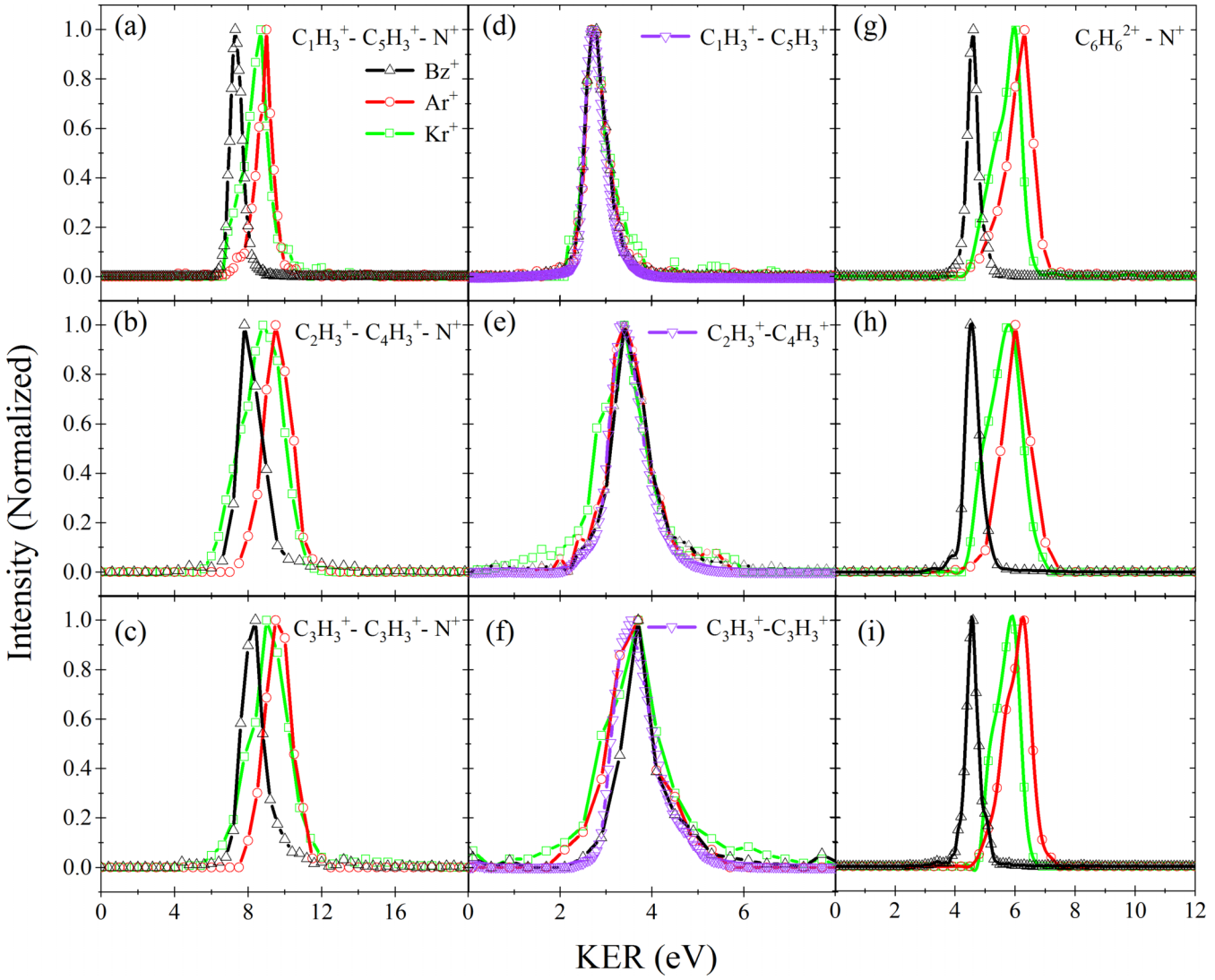

FIG. 3. The KER spectra of the three fragmentation channels from three dimers are presented in (a)–(c) for $C_6H_6^{2+}$ dissociation to $C_1H_3^+ + C_5H_3^+$, $C_2H_3^+ + C_4H_3^+$, and $C_3H_3^+ + C_3H_3^+$, respectively. The intramolecular KER spectra of the three channels are shown in (d)–(f), while the KER distribution of two-body channels without adjacency is indicated by the purple inverted triangle line. The intermolecular KER spectra for different adjacencies are depicted in (g)–(i), where the black triangle line, red point line, and green square line respectively represent $N =$ Bz, Ar, and Kr.

are presented in Figs. 2(a)–2(c), with the momenta of Bz^+ normalized to 1 a.u. (the normalization factor is 154 for three channels). The diagrams display two half-ring distributions, indicating that three-body CE in the dimer occurs via a sequential dissociation process, starting with the breakup of the dimer into two charged ions, $C_6H_6^{2+}$ and Bz^+, followed by the breaking up of $C_6H_6^{2+}$ into two fragments. The timescales of these two processes can differ significantly, with the repulsion between two charged Bz occurring within hundreds of femtoseconds [28,29], while the ring-breaking of $C_6H_6^{2+}$ requires tens to hundreds of nanoseconds [15]. In the ring breaking of the $C_6H_6^{2+}$, the initial step involves opening the carbon ring to a linear chain of six carbons, followed by various isomerization and fragmentation events. The fragments containing more than three carbons undergo ring closure processes, resulting in the production of several conformations [16]. During the CE process between two Bz^+ ions, repulsion between them induces rotational excitation. However, this effect is dissipated during the slow dissociation process, resulting in a circular distribution in the Newton diagrams as shown in Figs. 2(a)–2(c). The Newton diagrams for other dimers, such as C_6H_6-Ar and C_6H_6-Kr, display similar distributions because the rotation along with the slow ring-breaking process is only weakly affected by the CE between $C_6H_6^{2+}$ and other species.

In the meanwhile, the Dalitz plots [36] for three channels from the CE of $[C_6H_6 - Bz]^{3+}$ are shown in Figs. 2(d)–2(f). The coordinates in the plots are defined as

$$\begin{aligned} \text{Dalitz}_x &= (E_1 - E_2)/(\sqrt{3}W), \\ \text{Dalitz}_y &= E_3/W - 1/3, \end{aligned} \tag{4}$$

where E_1, E_2 are the kinetic energy of fragments from the second step dissociation, E_3 is the kinetic energy of molecular

cation from the first dissociation step, and $W = E_1 + E_2 + E_3$. Typically, when a sequential fragmentation channel occurs, there will be observable energy correlations between the fragments. This correlation serves as a useful indicator for determining the sequential process [9,37]. Analysis of the Dalitz plots reveals that the energy distribution of the fragments originating from $C_6H_6{}^{2+}$ is typically aligned parallel to the x axis. This indicates that the fragments share the total kinetic energy, while energy sharing with neighboring ions is negligible.

Figure 3 displays the measured KER spectra of the three-body CE channels from the three dimers. The total KER spectra for channels (1)–(3), which dissociate to $C_1H_3{}^+ + C_5H_3{}^+ + N^+$(N represents the neighbors Bz, Ar, and Kr), are shown in Fig. 3(a), with peak energies at 7.4, 8.9, and 8.5 eV, respectively. Figure 3(b) shows channels of $C_2H_3{}^+ + C_4H_3{}^+ + N^+$ with KER peaks at 8.1, 9.5, and 8.8 eV. Similarly, Fig. 3(c) shows KER peaks at 8.2, 9.5, and 9.2 eV for $C_3H_3{}^+ + C_3H_3{}^+ + N^+$. The peak values are obtained by fitting the measured KER spectra with a Gaussian function. Notably, the total KER for the same ring-breaking channel with three neighbors varied significantly, as it can be assigned as the KER between two parent ions and the KER from the ring-breaking of $C_6H_6{}^{2+}$ in a sequential fragmentation process, i.e., KER from inter- and intramolecular fragmentation, can be given as

$$\mathrm{KER_{total}} = \mathrm{KER_{inter}} + \mathrm{KER_{intra}}. \tag{5}$$

The total KER can be separated into two components since there is no energy correlation between neighbor ions and the other two fragments from $C_6H_6{}^{2+}$. The KER from the breaking of $C_6H_6{}^{2+}$ and the adjacent neighbor ions is referred to as $\mathrm{KER_{intra}}$ and is determined by multiplying the momentum of each fragment ion and dividing by the reduced mass. The difference between the total KER and $\mathrm{KER_{intra}}$ gives the $\mathrm{KER_{inter}}$ component. The KERs from the ring breaking of $C_6H_6{}^{2+}$ with and without neighbor ions are shown in Figs. 3(d)–3(f), with peak energies of 2.8 eV for $C_1H_3{}^+ + C_5H_3{}^+$, 3.5 eV for $C_2H_3{}^+ + C_4H_3{}^+$, and 3.7 eV for $C_3H_3{}^+ + C_3H_3{}^+$. No significant neighbor effects on $\mathrm{KER_{intra}}$ have been observed, and these values agree with previous measurements from isolated molecules [19,32]. KERs from intermolecular fragmentation are presented in Figs. 3(g)–3(i), with a noticeable difference observed when three neighbor ions are adjacent. The most probable value of $\mathrm{KER_{inter}}$ is around 4.6, 6.0, and 5.6 eV when neighbor ions are Bz^+, Ar^+, and Kr^+, respectively. The distance between ions, which is related to the initial stable structures as depicted in Fig. 1(b), is the most significant factor affecting the KER from CE of a dimer. The distances between the mass centers of the molecules and atoms for the three dimers are computed at the MP2 level with the aug-cc-pVDZ basis set using GAUSSIAN 09 [38]. The most stable structures of the three dimers are selected, and the distances R_1, R_2, and R_3 between the C_6H_6 molecule and Bz, Ar, Kr are found to be 4.8, 3.4, and 3.5 Å, respectively. Consequently, the KER obtained from a CE approximation can be approximated by KER $\sim 1/R$, leading to different $\mathrm{KER_{inter}}$ values observed in the measurements. The total KERs from inter- and intramolecular fragmentation for the three channels from the three dimers are summarized in Table I.

TABLE I. KER of Coulomb explosion channels from molecules and dimers.

Channel	Total KER (eV)	KER from Bz^{2+} breaking (eV)	
	This work		Reference
$C_1H_3{}^+ + C_5H_3{}^+$		2.8	3.0[a] 2.8[b] 2.9[c]
$C_1H_3{}^+ + C_5H_3{}^+ + Bz^+$	7.4	2.8	
$C_1H_3{}^+ + C_5H_3{}^+ + Ar^+$	8.9	2.8	
$C_1H_3{}^+ + C_5H_3{}^+ + Kr^+$	8.5	2.8	
$C_2H_3{}^+ + C_4H_3{}^+$		3.4	3.8[a] 3.3[b] 3.2[c]
$C_2H_3{}^+ + C_4H_3{}^+ + Bz^+$	8.1	3.5	
$C_2H_3{}^+ + C_4H_3{}^+ + Ar^+$	9.5	3.5	
$C_2H_3{}^+ + C_4H_3{}^+ + Kr^+$	8.8	3.7	
$C_3H_3{}^+ + C_3H_3{}^+$		3.6	4.2[a] 3.5[b] 3.5[c]
$C_3H_3{}^+ + C_3H_3{}^+ + Bz^+$	8.2	3.7	
$C_3H_3{}^+ + C_3H_3{}^+ + Ar^+$	9.5	3.6	
$C_3H_3{}^+ + C_3H_3{}^+ + Kr^+$	9.2	3.7	
$Bz^{2+} + Bz^+$	4.6		5.1 ± 0.4[d]
$Bz^{2+} + Ar^+$	6.0		6.7 ± 0.8[d]
$Bz^{2+} + Kr^+$	5.6		

[a]Taken from Ref. [15].
[b]Taken from Ref. [32].
[c]Taken from Ref. [19].
[d]Taken from Ref. [29].

The sequential fragmentation of the three dimers can be divided into two distinct processes, with intermolecular breaking occurring first and ring breaking happening subsequently due to the extended lifetime of the corresponding dissociation states. The presence of a neighbor ion in the dimer can be utilized as a diagnostic tool to examine the lifetimes of the molecular dications (Bz^{2+}) resulting from the repelling that takes place during the CE process [4]. The dissociation of the benzene dication results in $C_1H_3{}^+ + C_5H_3{}^+$ via the contribution of $^1B_{1g}$, $^1E_{1g}$, and $^1B_{2g}$ states, while the $^1A_{1u}$ and $^3A_{1u}$ states occupy the dissociation channel leading to $C_2H_3{}^+ + C_4H_3{}^+$. Excitation to higher states ($^2E_{1u}$ and $^2B_{2u}$) is necessary for $C_3H_3{}^+ + C_3H_3{}^+$ dissociation.

Figure 4 illustrates the three-body sequential breakup process in the native frame method [39]. This diagram aims to investigate how the rotation of Bz changes during the breaking process by examining the impact of the lifetimes of the intermediates [4]. The diagram illustrates the angular distribution [θ_{12} defined in Fig. 4(d)] between $C_6H_6{}^{2+}$ and Bz^+, Ar^+, and Kr^+, which provides information on the degree of rotation of intermediates. Similar angular distributions are observed for the same channel from different adjacent neighbor ions, indicating long lifetimes of corresponding states (tens to hundreds of nanoseconds), which average the influence of different neighbor ions on rotational excitation. Thus, it generates a uniform angular distribution in its center of mass frame if the intermediate molecular fragment ($C_6H_6{}^{2+}$) rotates for long enough.

The presence of adjacent ions during the CE process is similar to a half-collision process. The Coulomb force between the adjacent ions and the two dissociated fragments results in the largest number of the two dissociated fragments distributed at 90°, and the distribution decreases from 90°

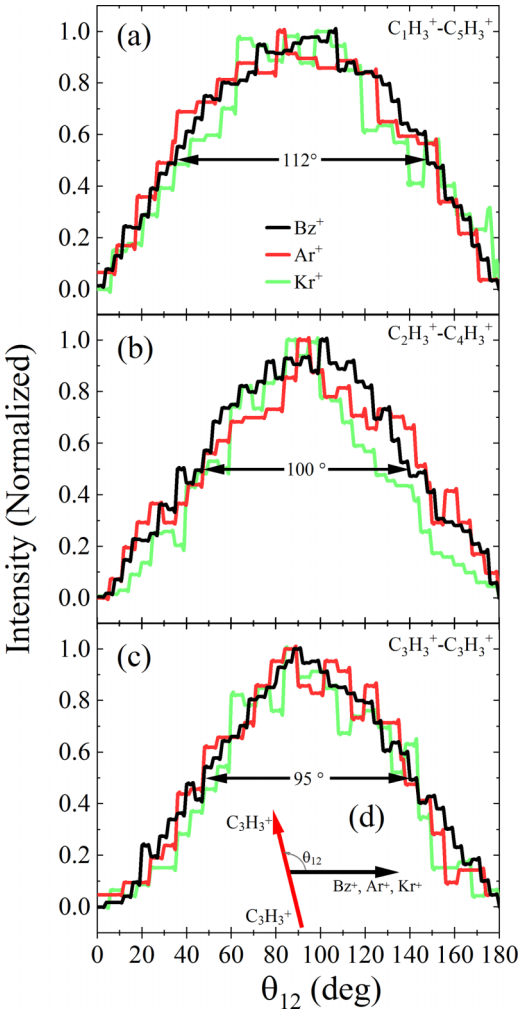

FIG. 4. (a)–(c) Angular distributions between the two fragmentation steps, i.e., intermolecular and intramolecular breaking, for three channels Bz^{2+} into $C_1H_3^+ + C_5H_3^+$, $C_2H_3^+ + C_4H_3^+$, and $C_3H_3^+ + C_3H_3^+$, respectively. The angle θ_{12} represents the angle between $C_6H_6^{2+}$ and the adjacent ion Bz^+ (black lines/black), Ar^+ (red lines/dark gray), or Kr^+ (green lines/light gray). The full width at half maximum is indicated beside each line. (d) shows the first and second dissociation steps of the three-body fragmentation process, with the angle θ_{12} between the two fragments denoted by black and red arrows.

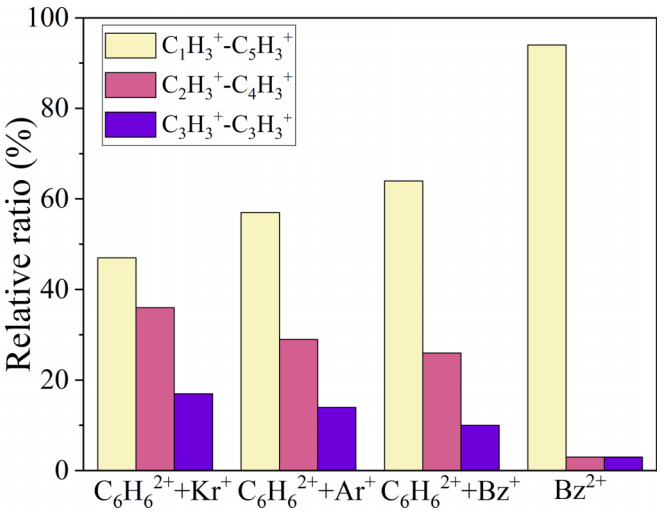

FIG. 5. The relative ratios of the dissociation channels from the three dimers. The dissociation channels correspond to $C_6H_6^{2+}$ dissociating to $C_1H_3^+ + C_5H_3^+$ (yellow/light gray), $C_2H_3^+ + C_4H_3^+$ (pink/middle gray), and $C_3H_3^+ + C_3H_3^+$ (purple/dark gray).

to 0° and 180°, which presents a symmetrical distribution. However, there is a noticeable difference in the full width at half maximum (FWHM) of the angular distributions between three channels. The FWHM of the angular distribution for channel $C_1H_3^+ + C_5H_3^+$ is 112°, wider than the other two channels, which are 100° and 95° for $C_2H_3^+ + C_4H_3^+$ and $C_3H_3^+ + C_3H_3^+$, respectively. The corresponding lifetimes for the states that produce these fragments are around 200 ns and 50 ns [15]. Thus, the angular distributions of fragments, when using neighbor ions as a reference, provide information on the lifetimes of states involved in the three-body sequential fragmentation.

The fragmentation of aromatic molecules and complexes is a subject of interest in astrochemistry, particularly with respect to products resulting from x-ray radiation or high-energy particle collisions [15,30,32,40]. The relative yields of the three two-body channels from dication states can vary considerably, with $C_1H_3^+ + C_5H_3^+$ being the most probable product from extreme ultraviolet (XUV) photon interactions [15] and $C_2H_3^+ + C_4H_3^+$ having the largest branching ratio in ion collision experiments [32]. In this study, we have investigated the relative ratios of these three two-body fragmentation channels following femtosecond IR laser interaction under different environmental conditions, and the results are presented in Fig. 5. Our measurements demonstrate that $C_1H_3^+ + C_5H_3^+$ remains the dominant product, regardless of the environment. The ionization yields of molecules are highly dependent on the ionization potential for different ionic states, with lower ionization potentials leading to higher yields. The appearance energy for $C_1H_3^+ + C_5H_3^+$ is 27.8 eV, which is much lower than the appearance energies for the other two channels (29.5 eV, 30.1 eV), consistent with the observed dominance of $C_1H_3^+ + C_5H_3^+$ in our experiment.

The ratio of the three channels in the fragmentation of $C_6H_6^{2+}$ is sensitive to the presence of neighboring ions, with the relative yield of $C_1H_3^+ + C_5H_3^+$ decreasing and the yields of the other two channels increasing. The nature of the ring-breaking process of $C_6H_6^{2+}$ is complex, with its multiple potential energy surfaces and transition states [16]. Additionally, intermolecular breaking of the three dimers induces vibrational excitation of the Bz ring, ranging from sub-eV to around 1 eV, with varying neighbor ions [29]. Therefore, the effect of neighbor ions during CE can be thought of as a half-collision process, in which the induced vibrational excitation alters the probabilities of generating the three channels. Therefore, the differences observed between the effects of the three different neighboring ions can be attributed to the vibrational excitation induced during the half-collision process. However, fully understanding how neighboring ions impact the fragmentation of $C_6H_6^{2+}$ requires detailed molecular dynamics simulations of the corresponding excited

states, which presents a challenging task for molecular physics and quantum chemistry.

IV. CONCLUSION

To summarize, we investigated the dynamics of ring breaking in $C_6H_6^{2+}$ with three neighboring ions (Bz^+, Ar^+, and Kr^+) using strong field ionization and coincidence measurement, and assigned three fragmentation channels. The results show that the dissociation process occurs sequentially, with intramolecular dissociation occurring first, followed by the breaking of the $C_6H_6^{2+}$ ring after a long delay time, and the KER of the two processes can be extracted for the three dimers. We also examined the influence of lifetimes between corresponding states for the three channels by using neighboring ions as a reference. Furthermore, we measured the relative ratio between the three channels in different surroundings and found that a half-collision between the CE and neighboring ions induces vibration excitation, which changes the relative ratio. Understanding the impact of neighboring ions on the dissociation dynamics of molecules can be valuable in studying biochemical reactions in clusters and the fragmentation of DNA and proteins in complex environments.

ACKNOWLEDGMENTS

This work was supported by the National Natural Science Foundation of China (Grants No. 12074143, No. 12004135, No. 12134005, and No. 92250306).

[1] J. D. Pickering, B. Shepperson, B. A. K. Hübschmann, F. Thorning, and H. Stapelfeldt, Phys. Rev. Lett. **120**, 113202 (2018).
[2] A. S. Chatterley, C. Schouder, L. Christiansen, B. Shepperson, M. H. Rasmussen, and H. Stapelfeldt, Nat. Commun. **10**, 133 (2019).
[3] X. Zhu, X. Hu, S. Yan, Y. Peng, W. Feng, D. Guo, Y. Gao, S. Zhang, A. Cassimi, J. Xu, D. Zhao, D. Dong, B. Hai, Y. Wu, J. Wang, and X. Ma, Nat. Commun. **11**, 2987 (2020).
[4] A. Méry, X. Fléchard, S. Guillous, V. Kumar, M. Lalande, J. Rangama, W. Wolff, and A. Cassimi, Phys. Rev. A **104**, 042813 (2021).
[5] E. Wang, X. Ren, and A. Dorn, Phys. Rev. Lett. **126**, 103402 (2021).
[6] A. Méry, A. N. Agnihotri, J. Douady, X. Fléchard, B. Gervais, S. Guillous, W. Iskandar, E. Jacquet, J. Matsumoto, J. Rangama, F. Ropars, C. P. Safvan, H. Shiromaru, D. Zanuttini, and A. Cassimi, Phys. Rev. Lett. **118**, 233402 (2017).
[7] X. Ding, M. Haertelt, S. Schlauderer, M. S. Schuurman, A. Y. Naumov, D. M. Villeneuve, A. R. W. McKellar, P. B. Corkum, and A. Staudte, Phys. Rev. Lett. **118**, 153001 (2017).
[8] X. Yu, X. Zhang, X. Hu, X. Zhao, D. Ren, X. Li, P. Ma, C. Wang, Y. Wu, S. Luo, and D. Ding, Phys. Rev. Lett. **129**, 023001 (2022).
[9] X. Yu, X. Zhao, Z. Wang, Y. Yang, X. Zhang, P. Ma, X. Li, C. Wang, X. Xu, C. Wang, D. Zhang, S. Luo, and D. Ding, Phys. Rev. A **104**, 053104 (2021).
[10] A. Méry, V. Kumar, X. Fléchard, B. Gervais, S. Guillous, M. Lalande, J. Rangama, W. Wolff, and A. Cassimi, Phys. Rev. A **103**, 042813 (2021).
[11] J. Zhou, C. He, M.-M. Liu, E. Wang, S. Jia, A. Dorn, X. Ren, and Y. Liu, Phys. Rev. Res. **3**, 023050 (2021).
[12] H. H. Kristensen, L. Kranabetter, C. A. Schouder, C. Stapper, J. Arlt, M. Mudrich, and H. Stapelfeldt, Phys. Rev. Lett. **128**, 093201 (2022).
[13] X. Li, X. Yu, P. Ma, X. Zhao, C. Wang, S. Luo, and D. Ding, Chin. Phys. B **31**, 103304 (2022).
[14] C. A. Schouder, A. S. Chatterley, J. D. Pickering, and H. Stapelfeldt, Annu. Rev. Phys. Chem. **73**, 323 (2022).
[15] P. J. Richardson, J. H. D. Eland, and P. Lablanquie, Org. Mass Spectrom. **21**, 289 (1986).
[16] S. Anand and H. B. Schlegel, J. Phys. Chem. A **109**, 11551 (2005).
[17] A. Matsuda, M. Fushitani, R. D. Thomas, V. Zhaunerchyk, and A. Hishikawa, J. Phys. Chem. A **113**, 2254 (2009).
[18] M. Alagia, P. Candori, S. Falcinelli, M. S. P. Mundim, F. Pirani, R. Richter, M. Rosi, S. Stranges, and F. Vecchiocattivi, J. Chem. Phys. **135**, 144304 (2011).
[19] M. Alagia, P. Candori, S. Falcinelli, M. S. P. Mundim, F. Pirani, R. Richter, M. Rosi, S. Stranges, and F. Vecchiocattivi, Phys. Chem. Chem. Phys. **13**, 8245 (2011).
[20] A. H. Winney, Y. F. Lin, S. K. Lee, P. Adhikari, and W. Li, Phys. Rev. A **93**, 031402(R) (2016).
[21] J. Zhou, Y. Li, Y. Wang, S. Jia, X. Xue, T. Yang, Z. Zhang, A. Dorn, and X. Ren, Phys. Rev. A **104**, 032807 (2021).
[22] E. Arunan, T. Emilsson, and H. S. Gutowsky, J. Chem. Phys. **101**, 861 (1994).
[23] M. O. Sinnokrot, E. F. Valeev, and C. D. Sherrill, J. Am. Chem. Soc. **124**, 10887 (2002).
[24] M. O. Sinnokrot and C. D. Sherrill, J. Phys. Chem. A **108**, 10200 (2004).
[25] M. Dehghany, J. Norooz Oliaee, M. Afshari, N. Moazzen-Ahmadi, and A. R. W. McKellar, J. Chem. Phys. **132**, 194303 (2010).
[26] K. Esteki, A. Barclay, A. McKellar, and N. Moazzen-Ahmadi, Chem. Phys. Lett. **713**, 65 (2018).
[27] X. Yu, Y. Liu, K. Deng, X. Zhang, P. Ma, X. Li, C. Wang, Z. Cui, S. Luo, and D. Ding, Phys. Rev. A **105**, 063105 (2022).
[28] X. Yu, X. Hu, J. Zhou, X. Zhang, X. Zhao, S. Jia, X. Xue, D. Ren, X. Li, Y. Wu, X. Ren, S. Luo, and D. Ding, Chin. Phys. Lett. **39**, 113301 (2022).
[29] X. Ren, J. Zhou, E. Wang, T. Yang, Z. Xu, N. Sisourat, T. Pfeifer, and A. Dorn, Nat. Chem. **14**, 232 (2022).
[30] J. Zhou, X. Yu, S. Luo, X. Xue, S. Jia, X. Zhang, Y. Zhao, X. Hao, L. He, C. Wang, D. Ding, and X. Ren, Nat. Commun. **13**, 5335 (2022).
[31] Y. Li, M. Li, T. Yang, Y. Wang, S. Jia, X. Liu, and Z. Xu, Chem. Phys. Lett. **553**, 111358 (2022).
[32] G. Veshapidze, H. Shiromaru, Y. Achiba, and N. Kobayashi, Int. J. Mass. Spectrom. **239**, 27 (2004).
[33] R. Dörner, V. Mergel, O. Jagutzki, L. Spielberger, J. Ullrich, R. Moshammer, and H. Schmidt-Böcking, Phys. Rep. **330**, 95 (2000).

[34] J. Ullrich, R. Moshammer, A. Dorn, R. Dörner, L. P. H. Schmidt, and H. Schmidt-Böcking, Rep. Prog. Phys. **66**, 1463 (2003).

[35] S. Luo, J. Liu, X. Li, D. Zhang, X. Yu, D. Ren, M. Li, Y. Yang, Z. Wang, P. Ma, C. Wang, J. Zhao, Z. Zhao, and D. Ding, Phys. Rev. Lett. **126**, 103202 (2021).

[36] I. Bediaga, I. I. Bigi, A. Gomes, G. Guerrer, J. Miranda, and A. C. dos Reis, Phys. Rev. D **80**, 096006 (2009).

[37] X. Zhao, T. Xu, X. Yu, D. Ren, X. Zhang, X. Li, P. Ma, C. Wang, D. Zhang, Q. Wang, X. Hu, S. Luo, Y. Wu, J. Wang, and D. Ding, Phys. Rev. A **103**, 053103 (2021).

[38] M. J. Frisch, G. W. Trucks, H. B. Schlegel, G. E. Scuseria, M. A. Robb, J. R. Cheeseman, G. Scalmani, V. Barone, B. Mennucci, G. A. Petersson, H. Nakatsuji, M. Caricato, X. Li, H. P. Hratchian, A. F. Izmaylov, J. Bloino, G. Zheng, J. L. Sonnenberg, M. Hada, M. Ehara, K. Toyota, R. Fukuda, J. Hasegawa, M. Ishida, T. Nakajima, Y. Honda, O. Kitao, H. Nakai, T. Vreven, J. A. Montgomery, Jr., J. E. Peralta, F. Ogliaro, M. Bearpark, J. J. Heyd, E. Brothers, K. N. Kudin, V. N. Staroverov, T. Keith, R. Kobayashi, J. Normand, K. Raghavachari, A. Rendell, J. C. Burant, S. S. Iyengar, J. Tomasi, M. Cossi, N. Rega, J. M. Millam, M. Klene, J. E. Knox, J. B. Cross, V. Bakken, C. Adamo, J. Jaramillo, R. Gomperts, R. E. Stratmann, O. Yazyev, A. J. Austin, R. Cammi, C. Pomelli, J. W. Ochterski, R. L. Martin, K. Morokuma, V. G. Zakrzewski, G. A. Voth, P. Salvador, J. J. Dannenberg, S. Dapprich, A. D. Daniels, O. Farkas, J. B. Foresman, J. V. Ortiz, J. Cioslowski, and D. J. Fox, *Gaussian 09*, Revision D.01 (Gaussian, Inc., Wallingford CT, 2013), https://gaussian.com/g09citation/.

[39] J. Rajput, T. Severt, B. Berry, B. Jochim, P. Feizollah, B. Kaderiya, M. Zohrabi, U. Ablikim, F. Ziaee, K. Raju P., D. Rolles, A. Rudenko, K. D. Carnes, B. D. Esry, and I. Ben-Itzhak, Phys. Rev. Lett. **120**, 103001 (2018).

[40] S. Ganguly, M. Gisselbrecht, P. Eng-Johnsson, R. Feifel, P.-A. Hervieux, Z. Alfaytarouni, R. F. Fink, S. Díaz-Tendero, A. R. Milosavljević, P. Rousseau, and S. Maclot, Phys. Chem. Chem. Phys. **24**, 28994 (2022).